

# Divergence-free cut finite element methods for Stokes flow<sup>☆</sup>

Thomas Frachon<sup>1</sup>, Erik Nilsson<sup>\*,1</sup>, Sara Zahedi<sup>1</sup>

---

## Abstract

We develop two unfitted finite element methods for the Stokes equations based on  $\mathbf{H}^{\text{div}}$ -conforming finite elements. The first method is a cut finite element discretization of the Stokes equations based on the Brezzi-Douglas-Marini elements and involves interior penalty terms to enforce tangential continuity of the velocity at interior edges in the mesh. The second method is a cut finite element discretization of a three-field formulation of the Stokes problem involving the vorticity, velocity, and pressure and uses the Raviart-Thomas space for the velocity. We present mixed ghost penalty stabilization terms for both methods so that the resulting discrete problems are stable and the divergence-free property of the  $\mathbf{H}^{\text{div}}$ -conforming elements is preserved also for unfitted meshes. We compare the two methods numerically. Both methods exhibit robust discrete problems, optimal convergence order for the velocity, and pointwise divergence-free velocity fields, independently of the position of the boundary relative to the computational mesh.

*Key words:* mass conservation, mixed finite element methods, unfitted, Stokes equations, cut finite element method, vorticity-velocity-pressure formulation

*2020 MSC:* 65N30, 65N85, 65N22

---

## 1. Introduction

Computational methods for simulations of incompressible fluids that fail to produce pointwise divergence-free velocity approximations may result in numerical solutions with large errors and instabilities [1]. In this paper our aim is to present unfitted finite element discretizations of the Stokes equations that produce pointwise divergence-free velocity approximations, independently of how the boundary is positioned relative the computational mesh.

Let  $\Omega \subset \mathbb{R}^2$  be an open bounded domain with a piecewise smooth boundary  $\partial\Omega$ , occupied by an incompressible fluid. Given a source  $\mathbf{f} \in \mathbf{L}^2(\Omega)$ , boundary data  $\mathbf{g} \in \mathbf{L}^2(\Omega)$ , and fluid viscosity  $\mu > 0$ , we seek fluid velocity  $\mathbf{u} : \Omega \rightarrow \mathbb{R}^2$  and pressure  $p : \Omega \rightarrow \mathbb{R}$  satisfying the Stokes equations:

$$-\operatorname{div}(\mu \nabla \mathbf{u} - p \mathbf{I}) = \mathbf{f} \text{ in } \Omega, \quad (1.1)$$

$$\operatorname{div} \mathbf{u} = 0 \text{ in } \Omega, \quad (1.2)$$

$$\mathbf{u} = \mathbf{g} \text{ on } \partial\Omega. \quad (1.3)$$

Unfitted discretizations can be an alternative to standard fitted finite element discretizations when the domain  $\Omega$  is complicated to mesh. For problems where the boundary  $\partial\Omega$  or interfaces (internal boundaries) are evolving unfitted discretizations, avoiding remeshing processes, can be of great interest, see e.g. [2, 3] for unfitted discretizations of two-phase flow problems.

---

<sup>☆</sup>This research was supported by the Swedish Research Council Grant No. 2018-05262 and the Wallenberg Academy Fellowship KAW 2019.0190.

\*Corresponding author

<sup>1</sup>Department of Mathematics, KTH Royal Institute of Technology, SE-100 44 Stockholm, Sweden (frachon@kth.se, erikni6@kth.se, sara.zahedi@math.kth.se).

For the Stokes equations Cut Finite Element Methods (CutFEM) with optimal rates of convergence of the approximate velocity and pressure have been developed, see e.g. [4, 5] for the Stokes interface problem and e.g. [6, 7] for the Stokes fictitious domain problem. It is by now well-known that unfitted discretizations may depending on the position of the boundary or the interface (an internal boundary) have stability issues. To ensure stability and well-posed discrete problems a popular choice in connection with CutFEM is to add ghost penalty terms [8] in the weak form, see for example the works mentioned above. The ghost penalty terms ensure that the condition number of the resulting matrix from the cut finite element discretization scales with mesh size as for the fitted finite element discretization, independent of how the boundary is positioned relative the mesh.

Developed cut finite element discretizations for the Stokes problem are mostly based on popular inf-sup stable element pairs such as the Taylor-Hood elements see [5], mini-elements [6], or the P1 iso P2-P1 elements [4] and do not result in pointwise divergence-free approximations. Recently, a cut finite element discretization based on the Scott-Vogelius pair was proposed in [9]. Standard mixed finite element discretizations using the Scott-Vogelius pair result in pointwise divergence-free velocity approximations. However, with the CutFEM presented in [9] the approximate velocity is pointwise divergence-free only outside a band around the unfitted boundary. In [10] we show, for the Darcy interface problem, that proper ghost penalty stabilization terms are necessary for cut finite element discretizations to preserve the divergence-free property of  $\mathbf{H}^{\text{div}}$ -conforming elements.

The construction of efficient divergence-free mixed finite element discretizations of the Stokes problem is not trivial, not even when the mesh is fitted to the boundary and especially not in three space dimensions. Several strategies exists, with their pros and cons, see e.g. [1] and references therein. A way to bypass the challenge of constructing conforming, inf-sup stable, and divergence-free elements is to develop discretizations based on  $\mathbf{H}^{\text{div}}$ -conforming elements. The Brezzi-Douglas-Marini (BDM) space and Raviart-Thomas (RT) space are two  $\mathbf{H}^{\text{div}}$ -conforming finite element spaces. Together with their appropriate pressure spaces they form inf-sup stable pairs for the Stokes equations. However, these spaces are non-conforming with respect to  $\mathbf{H}^1$ . One approach of handling the lack of smoothness of these spaces has been to modify the weak formulation using interior penalty terms as in discontinuous Galerkin methods to enforce tangential continuity across interior edges of the mesh[11, 12]. We utilize this strategy combined with new ghost penalty stabilization terms and develop a cut finite element discretization based on the BDM space for the velocity with

1. optimal rates of convergence of the approximate velocity and pressure
2. well-posed linear systems where the condition number of the system matrix scales as for fitted finite element discretizations
3. pointwise divergence-free velocity approximations

For some boundary conditions the vorticity-velocity-pressure formulation of the Stokes equations is beneficial [13, 14] and discretizations that fall into an appropriate de Rham complex has been developed for fitted meshes [14]. We also develop a cut finite element discretization for this three-field formulation based on the RT space for the velocity field such that the three properties above are fulfilled. The third property implies pressure-robustness for standard mixed finite element methods [1]. Numerical results indicate that this also holds for the proposed cut finite element methods.

The outline of the paper is as follows. In Section 2 we present two unfitted finite element discretizations for the Stokes problem (1.1)-(1.3) and show that the velocity approximations are pointwise divergence-free. In Section 3 we present results from numerical experiments and finally, in Section 4 we summarize our findings.

## 2. The numerical methods

We start by introducing the computational mesh, the macro-element partition, and the finite element spaces we need in order to discuss our numerical methods.

### 2.1. Mesh

Introduce a computational domain  $\Omega_0 \supseteq \Omega$  with polygonal boundary  $\partial\Omega_0$ . Let  $\{\mathcal{T}_{0,h}\}_h$  be a quasi-uniform family of simplicial meshes of  $\Omega_0$ . We denote by  $h$  the piecewise constant function that on element  $T$  is equal to  $h_T > 0$ , the diameter of  $T$ . Let  $\max_{T \in \mathcal{T}_{0,h}} h_T < h_0$  with  $h_0 \ll 1$  small. Note that

$$\Omega_0 = \bigcup_{K \in \mathcal{T}_{0,h}} K. \quad (2.1)$$

We call  $\mathcal{T}_{0,h}$  the background mesh, and from it we construct the active mesh

$$\mathcal{T}_h := \{T \in \mathcal{T}_{0,h} : |T \cap \Omega| > 0\} \quad (2.2)$$

on which we will define our finite element spaces. We define

$$\Omega_{\mathcal{T}_h} := \bigcup_{T \in \mathcal{T}_h} T. \quad (2.3)$$

Denote by  $\mathcal{E}_h$  the set of edges that are shared by two elements in  $\mathcal{T}_h$ . This set contains all edges except the ones on  $\partial\Omega_{\mathcal{T}_h}$ .

The background mesh  $\mathcal{T}_{0,h}$  conforms to the fixed polygonal boundary  $\partial\Omega_0$  but the active mesh  $\mathcal{T}_h$  does not need to conform to  $\partial\Omega$ . In particular we assume there is an unfitted part  $\phi \neq \Sigma \subset \partial\Omega$ , either such that  $\Sigma = \partial\Omega$  or  $\partial\Omega \setminus \Sigma \subset \partial\Omega_0$ . Let  $\mathcal{G}_h$  denote the set of elements intersected by the unfitted boundary  $\Sigma$ ,

$$\mathcal{G}_h = \{T \in \mathcal{T}_h : |\Sigma \cap T| > 0\}, \quad (2.4)$$

and let  $\mathcal{F}_h$  denote the set of edges in  $\mathcal{G}_h$  that are shared by two elements in  $\mathcal{T}_h$ . These sets are illustrated in Figure 2.1.

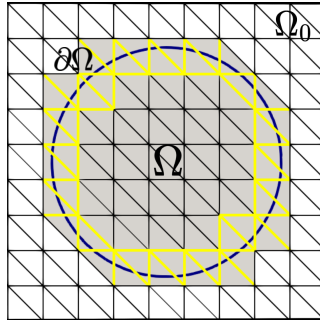


Figure 2.1: The grey domain is  $\Omega_{\mathcal{T}_h}$  and the yellow edges are edges in  $\mathcal{F}_h$ . Here  $\Sigma = \partial\Omega$ .

#### 2.1.1. Macro-elements

Given the active mesh we now construct a partition consisting of macro-elements with large  $\Omega$ -intersection [15]. Each element in the active mesh  $\mathcal{T}_h$  is classified either as having a large intersection with the domain  $\Omega$ , or a small intersection. We say that an element  $T \in \mathcal{T}_h$  has a large  $\Omega$ -intersection if

$$\delta \leq \frac{|T \cap \Omega|}{|T|}, \quad (2.5)$$

where  $\delta$  is a positive constant which is independent of the element and the mesh parameter. We collect all elements with a large intersection in

$$\mathcal{T}_H = \{T \in \mathcal{T}_h : |T \cap \Omega| \geq \delta|T|\}. \quad (2.6)$$

Using this classification we create a macro-element partition  $\mathcal{M}_h$  of  $\Omega_{\mathcal{T}_h}$ :

- To each  $T_L \in \mathcal{T}_H$  we associate a macro-element mesh  $\mathcal{T}_h(T_L)$  containing  $T_L$  and possibly adjacent elements that are in  $\mathcal{T}_h \setminus \mathcal{T}_H$ , i.e., elements classified as having a small intersection with  $\Omega$  and are connected to  $T_L$  via a bounded number of internal edges.
- Each element  $T \in \mathcal{T}_h$  belongs to precisely one macro-element mesh  $\mathcal{T}_h(T_L)$ .
- Each macro-element  $M_L \in \mathcal{M}_h$  is the union of elements in  $\mathcal{T}_h(T_L)$ , i.e.,

$$M_L = \bigcup_{T \in \mathcal{T}_h(T_L)} T. \quad (2.7)$$

We denote by  $\mathcal{F}_h(M)$  the set consisting of interior edges of  $M_L \in \mathcal{M}_h$ . Note that  $\mathcal{F}_h(M)$  is empty when  $T_L$  is the only element in  $\mathcal{T}_h(T_L)$ . See Figure 2.2 for an illustration of a macro-element partitioning. Edges in  $\mathcal{F}_h(M)$  are illustrated by dotted lines and black thick lines illustrate the boundary of macro-elements consisting of more than one element. We follow Algorithm 1 in [15] when we construct the macro-element partition.

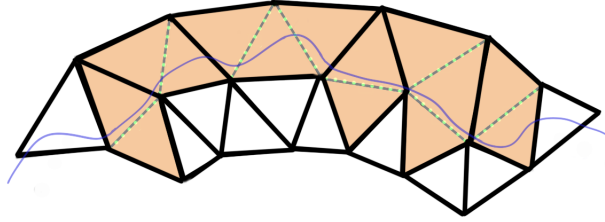


Figure 2.2: Illustration of a macro-element partition at the boundary  $\partial\Omega$ . Macro-elements consisting of more than one triangle are colored orange, separated by thick edges. Given a macro-element  $M \in \mathcal{M}_h$ , edges  $F \in \mathcal{F}_h(M)$  are illustrated by dotted lines.

## 2.2. Notation

We take the convention that the normal vector  $\mathbf{n}$  to  $\partial\Omega$  is outward pointing. We use the notation

$$(v, w)_D = \int_D v(\mathbf{x}) w(\mathbf{x}) \, d\mathbf{x} \quad (2.8)$$

for the  $L^2$ -inner product on a domain  $D \subset \mathbb{R}^2$ . The induced norm is denoted by  $\|\cdot\|_D$ .

We use identical notations for vector-valued functions and their associated spaces but those functions and spaces are represented using bold letters.

We will work with the Sobolev spaces

$$\mathbf{H}^1(D) := \{\mathbf{v} \in \mathbf{L}^2(D) : \nabla \mathbf{v} \in L^2(D)\}, \quad (2.9)$$

$$\mathbf{H}^{\text{div}}(D) := \{\mathbf{v} \in \mathbf{L}^2(D) : \text{div } \mathbf{v} \in L^2(D)\}, \quad (2.10)$$

$$H^1(D) := \{v \in L^2(D) : \nabla v \in L^2(D)\} \quad (2.11)$$

For a vector field  $\mathbf{u} = \begin{bmatrix} u_1 \\ u_2 \end{bmatrix}$  we set  $\text{curl } \mathbf{u} := \partial_2 u_1 - \partial_1 u_2$ , and for a scalar  $p$  we set  $\text{curl } p = \begin{bmatrix} -\partial_2 p \\ \partial_1 p \end{bmatrix}$ . Note that  $H^{\text{curl}}(D) := \{p \in L^2(D) : \text{curl } p \in L^2(D)\} \cong H^1(D)$ .

We introduce a unique normal  $\mathbf{n}$  to each edge  $F = \partial K_1 \cap \partial K_2$ , where  $K_1, K_2 \in \mathcal{T}_h$ . The normals of the edges on  $\partial\Omega_{\mathcal{T}_h}$  point outward. We define the tangent vector  $\mathbf{t}$  as the counter-clockwise rotation by  $\pi/2$  of  $\mathbf{n}$ . We define the jump and average operators of a scalar function  $p : \Omega_{\mathcal{T}_h} \rightarrow \mathbb{R}$  at  $F = \partial K_1 \cap \partial K_2$  by

$$[[p]] = (p_1 - p_2)|_F, \quad (2.12)$$

$$\{p\} = 1/2(p_1 + p_2)|_F, \quad (2.13)$$

where  $p_i = p|_{K_i}$ ,  $i = 1, 2$ . The same notation is used when considering jumps of vector-valued functions.

For two functions  $a, b$  we write  $a \lesssim b$  if and only if  $a \leq cb$  for some constant  $c$  independent of  $h$  and how the boundary  $\partial\Omega$  cuts the mesh  $\mathcal{T}_h$ . Similarly we write  $a \gtrsim b$ .

### 2.3. Spaces

Given an element  $T \in \mathcal{T}_h$ , let  $Q_k(T)$  denote the space of polynomial functions on  $T$  of degree less than or equal to  $k \geq 0$ . Let also  $\hat{k} = k$  or  $\hat{k} = k - 1$ . Define the following finite element spaces on the mesh  $\mathcal{T}_h$ :

$$W_{k+1,h} := \{\omega_h \in H^1(\Omega_{\mathcal{T}_h}) : \omega_h|_T \in Q_{k+1}(T), \forall T \in \mathcal{T}_h\}, \quad (2.14)$$

$$\mathbf{V}_{k,h} := \{\mathbf{v}_h \in \mathbf{H}^{\text{div}}(\Omega_{\mathcal{T}_h}) : \mathbf{v}_h|_T \in \mathbf{V}_k(T), \forall T \in \mathcal{T}_h\}, \quad (2.15)$$

$$Q_{\hat{k},h} := \bigoplus_{T \in \mathcal{T}_h} Q_{\hat{k}}(T). \quad (2.16)$$

Note that  $W_{k+1,h}$  is the standard space of continuous piecewise polynomials of degree less than or equal to  $k+1 \geq 1$ , while  $Q_{\hat{k},h}$  is the space of discontinuous piecewise polynomial functions. Here  $\mathbf{V}_k(T)$  is either the Raviart-Thomas space  $\mathbf{RT}_k(T)$  or the Brezzi-Douglas-Marini space  $\mathbf{BDM}_k(T)$ . These are the  $\mathbf{H}^{\text{div}}$ -conforming finite element spaces we choose for our velocity space. For the definition of these spaces we refer to for example Chapter III.3 in [16] or to [17]. Note that having chosen  $\mathbf{V}_{k,h}$  then  $\hat{k}$  is implicitly chosen. That is when  $\mathbf{V}_k = \mathbf{RT}_k$ , we take  $\hat{k} = k \geq 0$  and when  $\mathbf{V}_k = \mathbf{BDM}_k$ , we take  $\hat{k} = k - 1 \geq 0$ .

Before we state two discretizations for the Stokes problem, let us introduce two subspaces of our discrete spaces  $\mathbf{V}_{k,h}$  and  $Q_{\hat{k},h}$ .

$$\mathbf{V}_{k,h}^0 := \left\{ \mathbf{v}_h \in \mathbf{V}_{k,h} : \int_{\partial\Omega} \mathbf{v}_h \cdot \mathbf{n} = 0 \right\}, \quad (2.17)$$

$$Q_{\hat{k},h}^0 := \left\{ q_h \in Q_{\hat{k},h} : \int_{\Omega} q_h = 0 \right\}. \quad (2.18)$$

These spaces will be used to fix the non-uniqueness of the pressure variable when enforcing Dirichlet boundary conditions on the velocity, see (1.3). We will discuss this important aspect in Section 2.6.

### 2.4. A non-conforming mixed method

Functions in  $\mathbf{V}_{k,h}$  are tangentially discontinuous vector-valued functions, meaning that for  $\mathbf{v} \in \mathbf{V}_{k,h}$ ,  $\mathbf{v} \cdot \mathbf{t}$  is a discontinuous function across each edge in  $\mathcal{E}_h$ . The space  $\mathbf{V}_{k,h}$  lacks the smoothness to be conforming with respect to  $\mathbf{H}^1(\Omega_{\mathcal{T}_h})$ , meaning  $\mathbf{V}_{k,h} \not\subset \mathbf{H}^1(\Omega_{\mathcal{T}_h})$ . One approach of handling the lack of smoothness is to modify the weak formulation using interior penalty terms to enforce tangential continuity across interior edges of the mesh, see [11, 18]. Following this approach we now introduce an unstabilized unfitted discretization of the Stokes problem (1.1)-(1.3) as a starting point for a stabilized cut finite element method. The weak form reads: Find  $(\mathbf{u}_h, p_h) \in \mathbf{V}_{k,h} \times Q_{\hat{k},h}^0$  such that

$$a(\mathbf{u}_h, \mathbf{v}_h) - b(\mathbf{v}_h, p_h) = \mathcal{F}(\mathbf{v}_h) \text{ for all } \mathbf{v}_h \in \mathbf{V}_{k,h}^0, \quad (2.19)$$

$$b_0(\mathbf{u}_h, q_h) = 0, \text{ for all } q_h \in Q_{\hat{k},h}^0. \quad (2.20)$$

For  $\mathbf{u}_h, \mathbf{v}_h \in \mathbf{V}_{k,h}$ ,  $p_h, q_h \in Q_{\hat{k},h}$  the forms are defined as

$$a(\mathbf{u}_h, \mathbf{v}_h) := (\mu \nabla \mathbf{u}_h, \nabla \mathbf{v}_h)_\Omega - (\mu \nabla \mathbf{u}_h \cdot \mathbf{n}, \mathbf{v}_h)_{\partial\Omega} - (\mathbf{u}_h, \mu \nabla \mathbf{v}_h \cdot \mathbf{n})_{\partial\Omega} + (\lambda_u h^{-1} \mathbf{u}_h, \mathbf{v}_h)_{\partial\Omega} - t(\mathbf{u}_h, \mathbf{v}_h), \quad (2.21)$$

$$t(\mathbf{u}_h, \mathbf{v}_h) := \sum_{F \in \mathcal{E}_h} (\{ \mu \nabla(\mathbf{u}_h \cdot \boldsymbol{\tau}) \cdot \mathbf{n} \}, \llbracket \mathbf{v}_h \cdot \boldsymbol{\tau} \rrbracket)_F + (\llbracket \mathbf{u}_h \cdot \boldsymbol{\tau} \rrbracket, \{ \mu \nabla(\mathbf{v}_h \cdot \boldsymbol{\tau}) \cdot \mathbf{n} \})_F - (\lambda_t h^{-1} \llbracket \mathbf{u}_h \cdot \boldsymbol{\tau} \rrbracket, \llbracket \mathbf{v}_h \cdot \boldsymbol{\tau} \rrbracket)_F, \quad (2.22)$$

$$b(\mathbf{v}_h, p_h) := (\operatorname{div} \mathbf{v}_h, p_h)_\Omega - (\mathbf{v}_h \cdot \mathbf{n}, p_h)_{\partial\Omega}, \quad (2.23)$$

$$b_0(\mathbf{v}_h, p_h) := (\operatorname{div} \mathbf{v}_h, p_h)_\Omega, \quad (2.24)$$

$$\mathcal{F}(\mathbf{v}_h) := (\mathbf{f}, \mathbf{v}_h)_\Omega + (\lambda_u h^{-1} \mathbf{g}, \mathbf{v}_h)_{\partial\Omega} - (\mathbf{g}, \mu \nabla \mathbf{v}_h \cdot \mathbf{n})_{\partial\Omega}. \quad (2.25)$$

Here  $\lambda_t$  and  $\lambda_u$  are positive constants.

To derive this unstabilized method we multiply the Stokes problem with test functions  $(\mathbf{v}_h, q_h) \in \mathbf{V}_{k,h}^0 \times Q_{\hat{k},h}$ , apply integration by parts elementwise, and add terms in the weak form to make the bilinear form symmetric and to enforce tangential continuity weakly. We propose a stabilized unfitted finite element scheme by combining the weak form of the unstabilized method (2.19)-(2.20) with mixed ghost penalty stabilization terms developed in [10]. The finite element method which we refer to as Method NC (for non-conforming) reads: Find  $(\mathbf{u}_h, p_h) \in \mathbf{V}_{k,h} \times Q_{\hat{k},h}^0$  such that

$$\mathcal{A}(\mathbf{u}_h, \mathbf{v}_h) - \mathcal{B}(\mathbf{v}_h, p_h) = \mathcal{F}(\mathbf{v}_h), \quad \text{for all } \mathbf{v}_h \in \mathbf{V}_{k,h}^0, \quad (2.26)$$

$$\mathcal{B}_0(\mathbf{u}_h, q_h) = 0, \quad \text{for all } q_h \in Q_{\hat{k},h}. \quad (2.27)$$

Here

$$\mathcal{A}(\mathbf{u}_h, \mathbf{v}_h) := a(\mathbf{u}_h, \mathbf{v}_h) + s_a(\mathbf{u}_h, \mathbf{v}_h), \quad (2.28)$$

$$\mathcal{B}(\mathbf{u}_h, q_h) := b(\mathbf{u}_h, q_h) + s_b(\mathbf{u}_h, q_h), \quad (2.29)$$

$$\mathcal{B}_0(\mathbf{u}_h, q_h) := b_0(\mathbf{u}_h, q_h) + s_b(\mathbf{u}_h, q_h), \quad (2.30)$$

$$s_a(\mathbf{u}_h, \mathbf{v}_h) := \sum_{M \in \mathcal{M}_h} \sum_{F \in \mathcal{F}_h(M)} \sum_{j=0}^{\hat{k}+1} \tau_a h^{2j+\gamma_a} (\llbracket D_{\mathbf{n}_F}^j \mathbf{u}_h \rrbracket, \llbracket D_{\mathbf{n}_F}^j \mathbf{v}_h \rrbracket)_F, \quad (2.31)$$

$$s_b(\mathbf{u}_h, q_h) := \sum_{M \in \mathcal{M}_h} \sum_{F \in \mathcal{F}_h(M)} \sum_{j=0}^{\hat{k}} \tau_b h^{2j+1} (\llbracket D^j (\operatorname{div} \mathbf{u}_h) \rrbracket, \llbracket D^j q_h \rrbracket)_F, \quad (2.32)$$

where  $\llbracket D^j q_h \rrbracket$  denotes the jump in the generalised derivative of order  $j$  across the edge  $F$ . Similarly,  $\llbracket D_{\mathbf{n}_F}^j \mathbf{v}_h \rrbracket$  denotes the jump in the normal component of the generalised derivative, with  $\llbracket D_{\mathbf{n}_F}^0 \mathbf{v}_h \rrbracket = \llbracket \mathbf{v}_h \rrbracket$ . The stabilization parameters  $\tau_a > 0, \tau_b > 0$ , and we choose  $\gamma_a = -1$  for this method.

First note that the stabilized method also fits into the framework of non-symmetric saddle-point problems. The condition number of the associated linear system matrix to (2.26)-(2.27) is expected to scale like the condition number of the system matrix to a  $\mathbf{H}^{\operatorname{div}}$ -conforming boundary-fitted finite element method, see e.g. [19]. A similar remark holds regarding the approximation properties. Since our scheme is based on the boundary-fitted scheme of [11, 18], the convergence order of the pressure variable is expected to be optimal with respect to the larger pair  $\mathbf{BDM}_{k+1} \times Q_k$  but not with respect to the pair  $\mathbf{RT}_k \times Q_k$ . For the Raviart-Thomas space the method is only able to achieve a convergence in the pressure of order  $\hat{k}$ . See the a priori analysis in [11, 1] for details.

We now show that the proposed cut finite element method produces pointwise divergence-free approximations of solenoidal velocity fields, same as fitted standard FEM does with the considered element pairs. We follow the proof of [10]. Define the standard ghost penalty term for the pressure:

$$s_p(p_h, q_h) := \sum_{M \in \mathcal{M}_h} \sum_{F \in \mathcal{F}_h(M)} \sum_{j=0}^{\hat{k}} \tau_b h^{2j+\gamma} (\llbracket D^j p_h \rrbracket, \llbracket D^j q_h \rrbracket)_F. \quad (2.33)$$

**Theorem 1 (The divergence-free property).** *Assume  $\mathbf{u}_h \in \mathbf{V}_{k,h}$  satisfies (2.27), then  $\operatorname{div} \mathbf{u}_h = 0$ .*

PROOF. We have that  $\mathbf{u}_h \in \mathbf{V}_{k,h}$  satisfies

$$0 = \mathcal{B}_0(\mathbf{u}_h, q_h) = \int_{\Omega} \operatorname{div} \mathbf{u}_h q_h + \sum_{M \in \mathcal{M}_h} \sum_{F \in \mathcal{F}_h(M)} \sum_{j=0}^{\hat{k}} \tau_b h^{2j+1} ([D^j(\operatorname{div} \mathbf{u}_h)], [D^j q_h])_F, \quad \forall q_h \in Q_{\hat{k},h}.$$

We may choose  $q_h = \operatorname{div} \mathbf{u}_h$  since  $\operatorname{div} \mathbf{V}_{k,h} \subset Q_{\hat{k},h}$ . Then we have

$$0 = \|\operatorname{div} \mathbf{u}_h\|_{\Omega}^2 + s_p(\operatorname{div} \mathbf{u}_h, \operatorname{div} \mathbf{u}_h) \gtrsim \|\operatorname{div} \mathbf{u}_h\|_{\Omega_{\mathcal{T}_h}}^2 \geq 0, \quad (2.34)$$

where we used that for any  $q_h \in Q_{\hat{k},h}$ ,  $\|q_h\|_{\Omega}^2 + s_p(q_h, q_h) \gtrsim \|q_h\|_{\Omega_{\mathcal{T}_h}}^2$ , see Lemma 3.8 in [4] or Lemma 5.1 in [7]. We can thus conclude that  $\operatorname{div} \mathbf{u}_h = 0$  in  $\Omega_{\mathcal{T}_h}$ .

### 2.5. A conforming mixed vorticity method

It is convenient to introduce the following exact sequence

$$0 \hookrightarrow H^1(\Omega) \xrightarrow{\operatorname{curl}} \mathbf{H}^{\operatorname{div}}(\Omega) \xrightarrow{\operatorname{div}} L^2(\Omega) \rightarrow 0. \quad (2.35)$$

That the sequence is exact means that the kernel of a given operator in the sequence above is the image of the preceding operator in the same sequence. In particular, the divergence of the curl of a scalar field in 2D is 0 by virtue of the commutativity of  $x$ - and  $y$ -derivatives.

Let us introduce a new variable, the vorticity  $\omega := \mu \operatorname{curl} \mathbf{u}$ , and let  $\mathcal{H}(\Omega) := H^1(\Omega) \cong H^{\operatorname{curl}}(\Omega)$ . We make use of the incompressibility  $\operatorname{div} \mathbf{u} = 0$  to write  $-\operatorname{div}(\mu \nabla \mathbf{u}) = \operatorname{curl}(\mu \operatorname{curl} \mathbf{u}) - \nabla(\mu \operatorname{div} \mathbf{u}) = \operatorname{curl}(\mu \operatorname{curl} \mathbf{u})$ . The Stokes problem (1.1)-(1.3) becomes [13, 14]

$$\begin{cases} \mu^{-1} \omega - \operatorname{curl} \mathbf{u} = 0, & \text{in } \Omega, \\ \operatorname{curl} \omega + \nabla p = \mathbf{f}, & \text{in } \Omega, \\ \operatorname{div} \mathbf{u} = 0, & \text{in } \Omega, \\ \mathbf{u} = \mathbf{g}, & \text{on } \partial\Omega. \end{cases} \quad (2.36)$$

Multiplying the second equation of (2.36) with a test function  $\mathbf{v} \in \mathbf{H}^{\operatorname{div}}(\Omega)$  and integrating by parts we get

$$\int_{\Omega} \operatorname{curl} \omega \cdot \mathbf{v} + \int_{\partial\Omega} p \mathbf{v} \cdot \mathbf{n} - \int_{\Omega} p \operatorname{div} \mathbf{v} = \int_{\Omega} \mathbf{f} \cdot \mathbf{v}. \quad (2.37)$$

Multiplying the first equation of (2.36) with  $\tau \in \mathcal{H}(\Omega)$ , and integrating by parts we have

$$\int_{\Omega} \mu^{-1} \omega \tau - \int_{\Omega} \mathbf{u} \cdot \operatorname{curl} \tau = \int_{\partial\Omega} \mathbf{g} \cdot \mathbf{t} \tau. \quad (2.38)$$

Since the term  $-(\mathbf{u} \cdot \mathbf{t}, \tau)_{\partial\Omega}$  appears naturally in the integration by parts, we handle the boundary condition (1.3) such that the tangential component  $\mathbf{u} \cdot \mathbf{t}$  is treated as a natural boundary condition and the normal part  $\mathbf{u} \cdot \mathbf{n}$  is enforced weakly using Nitsche's method. The weak formulation of (2.36) reads as follows. Find  $(\omega, \mathbf{u}, p) \in \mathcal{H}(\Omega) \times \mathbf{H}^{\operatorname{div}}(\Omega) \times L^2(\Omega)$  such that

$$(\mu^{-1} \omega, \tau)_{\Omega} - (\mathbf{u}, \operatorname{curl} \tau)_{\Omega} = (\mathbf{g} \cdot \mathbf{t}, \tau)_{\partial\Omega}, \quad \forall \tau \in \mathcal{H}(\Omega), \quad (2.39)$$

$$(\operatorname{curl} \omega, \mathbf{v})_{\Omega} + (p, \mathbf{v} \cdot \mathbf{n})_{\partial\Omega} - (p, \operatorname{div} \mathbf{v})_{\Omega} = (\mathbf{f}, \mathbf{v})_{\Omega}, \quad \forall \mathbf{v} \in \mathbf{H}^{\operatorname{div}}(\Omega), \quad (2.40)$$

$$(\lambda \mathbf{u} \cdot \mathbf{n}, \mathbf{v} \cdot \mathbf{n})_{\partial\Omega} = (\lambda \mathbf{g} \cdot \mathbf{n}, \mathbf{v} \cdot \mathbf{n})_{\partial\Omega}, \quad \forall \mathbf{v} \in \mathbf{H}^{\operatorname{div}}(\Omega), \quad (2.41)$$

$$(\operatorname{div} \mathbf{u}, q) = 0, \quad \forall q \in L^2(\Omega). \quad (2.42)$$

Here  $\lambda \in L^{\infty}(\partial\Omega)$ .

### 2.5.1. The finite element method

We choose conforming finite element subspaces  $W_{k+1,h} \subset \mathcal{H}(\Omega)$ ,  $\mathbf{V}_{k,h} \subset \mathbf{H}^{\text{div}}(\Omega_{\mathcal{T}_h})$  with  $\mathbf{V}_k = \mathbf{RT}_k$ , and  $Q_{k,h} \subset L^2(\Omega_{\mathcal{T}_h})$ . These are the piecewise continuous polynomial functions of degree less than or equal to  $k+1$ , Raviart-Thomas elements, and piecewise discontinuous polynomial elements of degree less than or equal to  $k$ . To form our discrete formulation we add mixed ghost penalty stabilization terms. The method which we refer to as Method C (for conforming) reads: Find  $(\omega_h, \mathbf{u}_h, p_h) \in W_{k+1,h} \times \mathbf{V}_{k,h} \times Q_{k,h}^0$  for which

$$\mathcal{W}(\omega_h, \tau_h) - m(\tau_h, \mathbf{u}_h) = (\mathbf{g} \cdot \mathbf{t}, \tau_h)_{\partial\Omega}, \quad \forall \tau_h \in W_{k+1,h}, \quad (2.43)$$

$$\check{\mathcal{A}}(\mathbf{u}_h, \mathbf{v}_h) + m(\omega_h, \mathbf{v}_h) - \mathcal{B}(\mathbf{v}_h, p_h) = (\mathbf{f}, \mathbf{v}_h)_\Omega + (\lambda_{\mathbf{u}} h^{-1} \mathbf{g} \cdot \mathbf{n}, \mathbf{v}_h \cdot \mathbf{n})_{\partial\Omega}, \quad \forall \mathbf{v}_h \in \mathbf{V}_{k,h}^0, \quad (2.44)$$

$$\mathcal{B}_0(\mathbf{u}_h, q_h) = 0, \quad \forall q_h \in Q_{k,h}. \quad (2.45)$$

Here  $\mathcal{B}$  and  $\mathcal{B}_0$  are as in (2.29) and (2.30), and

$$w(\omega, \tau) := (\mu^{-1} \omega, \tau)_\Omega, \quad (2.46)$$

$$\mathcal{W}(\omega_h, \tau_h) := w(\omega_h, \tau_h) + s_w(\omega_h, \tau_h), \quad (2.47)$$

$$s_w(\omega_h, \tau_h) := \sum_{M \in \mathcal{M}_h} \sum_{F \in \mathcal{F}_h(M)} \sum_{j=1}^k \tau_w h^{2j+1} (\llbracket D_{\mathbf{n}_F}^j \omega_h \rrbracket, \llbracket D_{\mathbf{n}_F}^j \tau_h \rrbracket)_F, \quad (2.48)$$

$$m(\tau, \mathbf{v}) := (\mathbf{u}, \text{curl } \tau)_\Omega, \quad (2.49)$$

$$\check{a}(\mathbf{u}, \mathbf{v}) := (\lambda_{\mathbf{u}} h^{-1} \mathbf{u} \cdot \mathbf{n}, \mathbf{v} \cdot \mathbf{n})_{\partial\Omega}, \quad (2.50)$$

$$\check{\mathcal{A}}(\mathbf{u}_h, \mathbf{v}_h) := \check{a}(\mathbf{u}_h, \mathbf{v}_h) + s_a(\mathbf{u}_h, \mathbf{v}_h), \quad (2.51)$$

where  $\tau_w$  and  $\lambda_{\mathbf{u}}$  are positive sufficiently large constants. For this method we choose  $s_a$  as in equation (2.31) but with  $\gamma_a = 1$ . The stabilization terms are chosen so that we retain the structure of the original problem. One can remove the stabilization  $s_a$  but add a stabilization to  $m(\cdot, \cdot)$  by

$$\mathcal{M}(\tau_h, \mathbf{u}_h) := m(\tau_h, \mathbf{u}_h) + s_m(\tau_h, \mathbf{u}_h), \quad (2.52)$$

$$s_m(\tau_h, \mathbf{u}_h) := \sum_{M \in \mathcal{M}_h} \sum_{F \in \mathcal{F}_h(M)} \sum_{j=0}^k \tau_m h^{2j+1} (\llbracket D_{\mathbf{n}_F}^j (\text{curl } \tau_h) \rrbracket, \llbracket D_{\mathbf{n}_F}^j \mathbf{u}_h \rrbracket)_F. \quad (2.53)$$

These choices create different numerical methods which we label<sup>2</sup> as  $(\tau_w, \tau_m, \tau_a)$ , for instance our present choice is  $(\tau_w, 0, \tau_a)$ . Moreover, since (2.45) is the same equation as (2.27), Theorem 1 holds for Method C as well.

The discrete problem with Dirichlet boundary conditions (1.3) fails to fall into an appropriate de Rham complex. In [14], this is suggested to impact the theoretical convergence order of the pressure variable. However, when we choose appropriate stabilization terms, we do not notice this in our numerical experiments in Section 3. According to [14], the convergence order is provably optimal for fitted FEM with respect to either of the following boundary conditions

$$\omega \mathbf{t} = \omega_0 \mathbf{t}, \quad \mathbf{u} \cdot \mathbf{n} = u_0, \quad \text{or} \quad (2.54)$$

$$\mathbf{u} \cdot \mathbf{t} = u_0, \quad p = p_0. \quad (2.55)$$

We study the presented method with the boundary condition (2.55) in Section 3. Since there is no  $\check{a}$ -term for these boundary conditions we choose the following stabilization  $(0, \tau_m, 0)$ . Hence the weak form reads: Find  $(\omega_h, \mathbf{u}_h, p_h) \in W_{k+1,h} \times \mathbf{V}_{k,h} \times Q_{k,h}$  such that

$$w(\omega_h, \tau_h) - \mathcal{M}(\tau_h, \mathbf{u}_h) = (u_0, \tau_h)_{\partial\Omega}, \quad \forall \tau_h \in W_{k+1,h}, \quad (2.56)$$

$$\mathcal{M}(\omega_h, \mathbf{v}_h) - \mathcal{B}(\mathbf{v}_h, p_h) = (\mathbf{f}, \mathbf{v}_h)_\Omega - (p_0, \mathbf{v}_h \cdot \mathbf{n})_{\partial\Omega}, \quad \forall \mathbf{v}_h \in \mathbf{V}_{k,h}, \quad (2.57)$$

$$\mathcal{B}_0(\mathbf{u}_h, q_h) = 0, \quad \forall q_h \in Q_{k,h}. \quad (2.58)$$

<sup>2</sup>The  $s_b$  stabilization is always included, whence  $\tau_b$  is not included in the label.



**Remark 1 (The three-dimensional case).** The description of the method changes only slightly when going up one dimension to 3D. The exact sequence picks up an extra intermediate space:

$$[2D] \quad 0 \hookrightarrow H^1(\Omega) \xrightarrow{\text{curl}} \mathbf{H}^{\text{div}}(\Omega) \xrightarrow{\text{div}} L^2(\Omega) \rightarrow 0 \quad (2.59)$$

$$[3D] \quad 0 \hookrightarrow H^1(\Omega) \xrightarrow{\nabla} \mathbf{H}^{\text{curl}}(\Omega) \xrightarrow{\text{curl}} \mathbf{H}^{\text{div}}(\Omega) \xrightarrow{\text{div}} L^2(\Omega) \rightarrow 0 \quad (2.60)$$

Setting  $\mathcal{H}(\Omega) := \mathbf{H}^{\text{curl}}(\Omega)$  with  $\text{curl } \mathbf{u} := \nabla \times \mathbf{u}$ , the method reads identically up to changing edges to faces and  $\mathbf{v} \cdot \mathbf{t} \mapsto \mathbf{n} \times \mathbf{v}$ . One exchanges  $W_{k+1,h}$  with vector-valued Nédélec edge elements of the first kind, see [20, 21].

The boundary conditions (2.54) and (2.55) change to

$$\mathbf{n} \times \boldsymbol{\omega} = \boldsymbol{\omega}_0, \quad \mathbf{u} \cdot \mathbf{n} = u_0, \quad \text{or} \quad (2.61)$$

$$\mathbf{n} \times \mathbf{u} = \mathbf{u}_0, \quad p = p_0. \quad (2.62)$$

We believe that the above natural changes would make our presented method work for 3D as well. However, we have only implemented the method in 2D at present.

### 2.6. On the impact of Lagrange multipliers

We focus our discussion in this subsection on Method NC (presented in Section 2.4) but everything carries over to Method C (see Section 2.5).

With the boundary condition (1.3) one runs into the well-known issue that the pressure is only determined up to a constant. Specifically, this happens in boundary-fitted FEM, as well as CutFEM, since an integration by parts reveals that the kernel of  $b$ , respectively  $\mathcal{B}$ , is non-empty and consists of the constant functions in bijection with  $\mathbb{R}$ . Determining this unknown constant is usually handled by modifying the trial pressure space by setting the mean value:

$$Q_{\hat{k},h}^0 = \left\{ q_h \in \bigoplus_{T \in \mathcal{T}_h} Q_{\hat{k}}(T) : \int_{\Omega} q_h = 0 \right\}. \quad (2.63)$$

The space (2.63) is difficult to work with numerically (see [17, Section 5.2.5]), so equivalently one adds a Lagrange multiplier  $\sigma \in \mathbb{R}$  such that  $\sigma \int_{\Omega} p_h$  is added to the corresponding minimization problem of (2.26)-(2.27). Then the resulting discrete variational system has an additional variable  $\chi$ , and we search for solutions  $(\mathbf{u}_h, p_h, \chi) \in \mathbf{V}_{k,h} \times Q_{\hat{k},h} \times \mathbb{R}$  to

$$\begin{aligned} \mathcal{A}(\mathbf{u}_h, \mathbf{v}_h) - \mathcal{B}(\mathbf{v}_h, p_h) &= \mathcal{F}(\mathbf{v}_h) \text{ for all } \mathbf{v}_h \in \mathbf{V}_{k,h}, \\ \mathcal{B}_0(\mathbf{u}_h, q_h) + (\chi, q_h)_{\Omega} &= 0 \text{ for all } q_h \in Q_{\hat{k},h}, \\ (\sigma, p_h)_{\Omega} &= 0, \quad \sigma \in \mathbb{R}. \end{aligned} \quad (2.64)$$

Importantly, the divergence condition changes and it is easy to see that we are solving

$$\text{div } \mathbf{u}_h = -\chi. \quad (2.65)$$

In standard FEM where the mesh is fitted to the boundary  $\partial\Omega$ , equation (2.65) is not an issue, because  $\chi$  will be 0. However for our unfitted FEM, we have noticed that  $\chi$  is typically *not* 0. In unfitted FEM where the property  $\text{div } \mathbf{V}_{k,h} \subset Q_{\hat{k},h}$  does not hold, this is not noticed since  $\chi \rightarrow 0$  as  $h \rightarrow 0$ .

Let us investigate what happens to  $\chi$ . Recall that the magnitude of a Lagrange multiplier is a representation of how hard it is for the system to deal with the corresponding constraint. For  $q_h \in \mathbb{R}$ ,

$$\mathcal{B}_0(\mathbf{u}_h, q_h) + (\chi, q_h)_{\Omega} = 0 \quad (2.66)$$

$$\implies 0 = \int_{\partial\Omega} \mathbf{u}_h \cdot \mathbf{n} + \int_{\Omega} \chi \implies |\Omega| \chi = - \int_{\partial\Omega} \mathbf{g} \cdot \mathbf{n}, \quad (2.67)$$

where we have used integration by parts. For fitted FEM, imposing the boundary condition  $\mathbf{u}_h \cdot \mathbf{n}|_{\partial\Omega} = \mathbf{g} \cdot \mathbf{n}$  strongly, with  $\int_{\partial\Omega} \mathbf{g} \cdot \mathbf{n} = 0$  as a compatibility criterion on the datum  $\mathbf{g}$ , implies  $\chi = 0$  for a well-posed problem. For unfitted FEM, imposing the boundary condition weakly yields  $\int_{\partial\Omega} \mathbf{u}_h \cdot \mathbf{n} \approx \int_{\partial\Omega} \mathbf{g} \cdot \mathbf{n}$ . The result is that it is harder to set  $\int_{\Omega} p_h = 0$  with a Lagrange multiplier in the unfitted setting, so  $\chi \neq 0$ .

Below we present one solution to how to get a unique pressure without destroying the divergence condition.

### 2.6.1. Mixed Lagrange multipliers

When imposing boundary conditions strongly in fitted FEM we set  $\mathbf{v}_h \cdot \mathbf{n} = 0$  in the space of the test functions. The idea is that we are lacking this criterion when the mesh is not fitted. So we pair  $\int_{\Omega} p_h = 0$  with a linear equation on the DOFs of the test space  $\mathbf{V}_{k,h}$ ; namely  $\int_{\partial\Omega} \mathbf{v}_h \cdot \mathbf{n} = 0$ . We have already written our methods with this in mind by using  $\mathbf{V}_{k,h}^0$  and  $Q_{k,h}^0$ , but let us show how Method NC and Method C are written in terms of the Lagrange multipliers.

Method NC reads: Find  $(\mathbf{u}_h, p_h, \chi) \in \mathbf{V}_{k,h} \times Q_{k,h} \times \mathbb{R}$  for which

$$\begin{aligned} \mathcal{A}(\mathbf{u}_h, \mathbf{v}_h) + \mathcal{B}(\mathbf{v}_h, p_h) + (\chi, \mathbf{v}_h \cdot \mathbf{n})_{\partial\Omega} &= \mathcal{F}(\mathbf{v}_h), & \text{for all } \mathbf{v}_h \in \mathbf{V}_{k,h}, \\ \mathcal{B}_0(\mathbf{u}_h, q_h) &= 0, & \text{for all } q_h \in Q_{k,h}, \\ (\sigma, p_h)_{\Omega} &= 0, & \sigma \in \mathbb{R}. \end{aligned} \quad (2.68)$$

Expanding trial and test functions in their finite element basis, let  $\hat{\mathbf{f}}$  be the data vector corresponding to  $\mathcal{F}$  and let  $\begin{bmatrix} \hat{\mathbf{u}} \\ \hat{\mathbf{p}} \end{bmatrix}$  denote the unknown degree of freedom (DOF) values. The linear system of equations associated with (2.68) can be written as

$$\begin{bmatrix} \mathbf{A} & -\mathbf{B}^T & (1, \mathbf{v}_h \cdot \mathbf{n})_{\partial\Omega} \\ \mathbf{B}_0 & \mathbf{0} & \mathbf{0} \\ 0 & (1, \sigma)_{\Omega} & 0 \end{bmatrix} \begin{bmatrix} \hat{\mathbf{u}} \\ \hat{\mathbf{p}} \\ \xi \end{bmatrix} = \begin{bmatrix} \hat{\mathbf{f}} \\ \mathbf{0} \\ 0 \end{bmatrix}. \quad (2.69)$$

Method C reads: Find  $(\omega_h, \mathbf{u}_h, p_h, \chi) \in W_{k+1,h} \times \mathbf{V}_{k,h} \times Q_{k,h} \times \mathbb{R}$  for which

$$\begin{aligned} \mathcal{W}(\omega_h, \boldsymbol{\tau}_h) - \mathcal{M}(\boldsymbol{\tau}_h, \mathbf{u}_h) &= (\mathbf{g} \cdot \boldsymbol{\tau}, \boldsymbol{\tau}_h)_{\partial\Omega}, & \forall \boldsymbol{\tau}_h \in W_{k+1,h}, \\ \check{\mathcal{A}}(\mathbf{u}_h, \mathbf{v}_h) + \mathcal{M}(\omega_h, \mathbf{v}_h) - \mathcal{B}(\mathbf{v}_h, p_h) + (\chi, \mathbf{v}_h \cdot \mathbf{n})_{\partial\Omega} &= (\mathbf{f}, \mathbf{v}_h)_{\Omega} + (\lambda_{\mathbf{u}} h^{-1} \mathbf{g} \cdot \mathbf{n}, \mathbf{v}_h \cdot \mathbf{n})_{\partial\Omega}, & \forall \mathbf{v}_h \in \mathbf{V}_{k,h}, \\ \mathcal{B}_0(\mathbf{u}_h, q_h) &= 0, & \forall q_h \in Q_{k,h}, \\ (\sigma, p_h)_{\Omega} &= 0, & \sigma \in \mathbb{R}. \end{aligned} \quad (2.70)$$

The linear system of equations associated with (2.70) can be written as

$$\begin{bmatrix} \mathbf{W} & -\mathbf{M}^T & \mathbf{0} & \mathbf{0} \\ \mathbf{M} & \check{\mathbf{A}} & -\mathbf{B}^T & (1, \mathbf{v}_h \cdot \mathbf{n})_{\partial\Omega} \\ \mathbf{0} & \mathbf{B}_0 & \mathbf{0} & \mathbf{0} \\ 0 & 0 & (1, \sigma)_{\Omega} & 0 \end{bmatrix} \begin{bmatrix} \hat{\omega} \\ \hat{\mathbf{u}} \\ \hat{\mathbf{p}} \\ \xi \end{bmatrix} = \begin{bmatrix} \hat{\mathbf{g}} \\ \hat{\mathbf{f}} \\ \mathbf{0} \\ 0 \end{bmatrix}. \quad (2.71)$$

Note that the divergence condition isn't disturbed for either method, so nothing changes in the proof of Theorem 1.

## 3. Numerical Experiments

In this section we study the performance of the proposed methods. The source code for all numerical simulations is available at [22]. Specifically, we highlight that incompressibility (1.2) is preserved when pure Dirichlet boundary conditions are imposed. We illustrate that both methods are pressure-robust by considering an example introduced in [1]. We show how imposition of the pressure mean via a standard Lagrange multiplier as well as standard ghost penalty stabilization for the pressure result in erroneous divergence. We

also study mixed boundary conditions of type (2.55) and show that Method C exhibits optimal convergence and condition number scaling.

For short-hand we will in this Section write  $P_{k+1}$  for the continuous piecewise polynomial space  $W_{k+1,h}$ ,  $\mathbf{RT}_k$  for  $\mathbf{V}_{k,h}$  with  $\mathbf{V}_k(T) = \mathbf{RT}_k(T)$ ,  $\mathbf{BDM}_k$  for  $\mathbf{V}_{k,h}$  with  $\mathbf{V}_k(T) = \mathbf{BDM}_k(T)$ , and  $Q_k$  for the space of discontinuous polynomials  $Q_{k,h}$ .

In all the examples we compute the condition number of the system matrix using MATLAB's *condst* function, which computes a lower bound for the 1-norm condition number. All linear systems are solved using a direct solver, either UMFPACK or MUMPS, and we state when we use which.

Note that in general we do not have the exact boundary  $\partial\Omega$  but rather an approximation  $(\partial\Omega)_h$ . In the implementation of all the schemes, we replace  $\partial\Omega$  by a piecewise linear approximation  $(\partial\Omega)_h$ . Consequently, we also have an approximation  $\Omega_h$  of  $\Omega$ .

### 3.1. Example 1 - Homogeneous Dirichlet BC

Consider the example from [9]. The domain  $\Omega$  is the disk of radius 0.5 centered at (0.5, 0.5), and the exact solution to the Stokes problem is

$$\mathbf{u}(x, y) = \begin{pmatrix} 2((x-0.5)^2 + (y-0.5)^2 - 0.25)(2y-1) \\ 2((x-0.5)^2 + (y-0.5)^2 - 0.25)(2x-1) \end{pmatrix}, \quad p(x, y) = 10(x^2 - y^2)^2. \quad (3.1)$$

We embed  $\Omega \subset \Omega_0 := [0, 1]^2$ , so it becomes a fictitious domain problem. We use a uniform background mesh. We study this problem also in subsections 3.1.1, 3.1.2, and 3.1.3, but from different angles. For both methods we take a macro-stabilization parameter  $\delta = 1$  and Nitsche penalty parameter  $\lambda_{\mathbf{u}} = 4 \cdot 10^3$ . For Method NC we take  $\lambda_t = 1/100$ ,  $\tau_a = \tau_b = \lambda_t$ . For Method C we take  $\tau_a = \tau_b = \tau_w = 10$ .

The main comparison in this subsection will be between Method C and Method NC. For Method NC we include both pairs  $\mathbf{RT}_1 \times Q_1$  and  $\mathbf{BDM}_1 \times Q_0$ . We also compare with the corresponding unstabilized discretizations. From Figure 3.1 we see that for both methods, the velocity convergence is second order, which

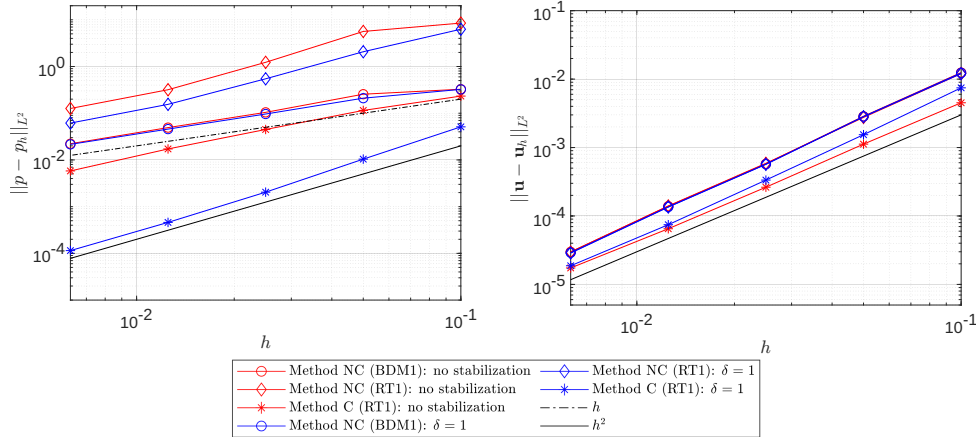


Figure 3.1: Example 1: Method NC ( $\mathbf{BDM}_1 \times Q_0$ ,  $\mathbf{RT}_1 \times Q_1$ ) vs. Method C ( $P_2 \times \mathbf{RT}_1 \times Q_1$ ), pressure and velocity errors. Left: The  $L^2$ -error of the pressure versus mesh size  $h$ . Right: The  $L^2$ -error of the velocity field versus mesh size  $h$ .

is optimal. The left panel in Figure 3.1 shows that Method NC with the pair  $\mathbf{RT}_1 \times Q_1$  suffers from suboptimal convergence of the pressure, as expected, while with the larger pair  $\mathbf{BDM}_1 \times Q_0$  the pressure convergence is optimal, i.e., of order 1. It is surprising that Method C achieves pressure convergence of order 2 in this example. We also observe that both stabilized methods always perform better than their corresponding unstabilized version. In Figure 3.2 we see that the condition number of the stabilized methods scale optimally

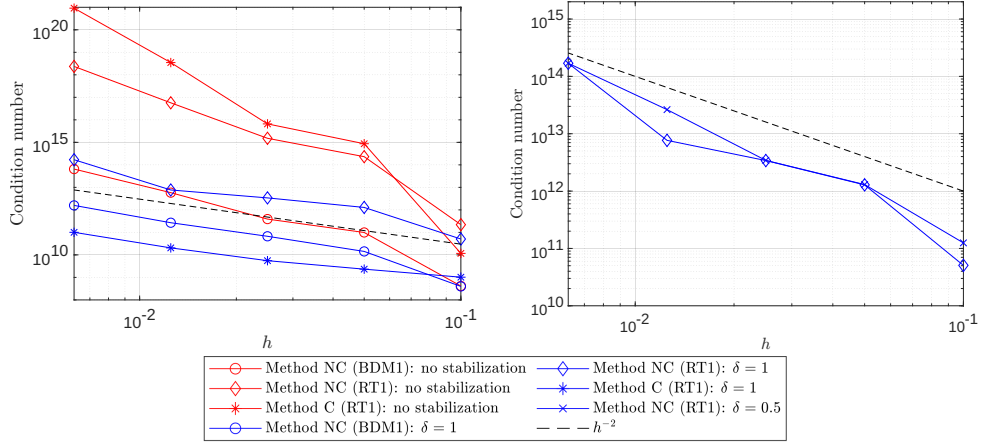


Figure 3.2: Example 1: Method NC ( $\mathbf{BDM}_1 \times Q_0$ ,  $\mathbf{RT}_1 \times Q_1$ ) vs. Method C ( $P_2 \times \mathbf{RT}_1 \times Q_1$ ), condition numbers. Left: The 1-norm condition number versus mesh size  $h$ . Right: The 1-norm condition number versus mesh size  $h$ , comparing  $\delta = 0.5$  with  $\delta = 1$  for highest order Method NC.

as  $O(h^{-2})$ . For the  $\mathbf{RT}_1$ -elements we see that stabilization is really necessary to control the condition number. In the right panel of Figure 3.2 the condition number of Method NC is shown for the pair  $\mathbf{RT}_1 \times Q_1$  with  $\delta = 0.5$  and  $\delta = 1$ . We observe an  $O(h^{-2})$  scaling.

$h$	Method NC (BDM1): No stabilization	Method NC (BDM1): $\delta = 1$	Method NC (RT1): No stabilization	Method NC (RT1): $\delta = 1$	Method C (RT1): No stabilization	Method C (RT1): $\delta = 1$
0.1	1.25037e-15	6.52568e-16	2.99904e-15	1.98797e-15	1.84033e-15	2.40234e-13
0.05	2.48203e-15	1.45681e-15	8.89057e-15	3.54505e-15	3.47963e-15	3.04883e-13
0.025	7.48215e-15	3.61401e-15	1.9477e-14	6.78915e-15	6.78857e-15	2.18917e-13
0.0125	2.35407e-14	6.19408e-15	7.12774e-14	1.36284e-14	1.3676e-14	1.72203e-13
0.00625	9.48173e-14	2.68222e-13	1.92617e-13	4.95346e-13	2.39412e-11	2.31925e-11

Table 3.1:  $L^2$ -error of divergence for different mesh sizes  $h$ .

$h$	Method NC (BDM1): no stabilization	Method NC (BDM1): $\delta = 1$	Method NC (RT1): no stabilization	Method NC (RT1): $\delta = 1$	Method C (RT1): no stabilization	Method C (RT1): $\delta = 1$
0.1	5.10703e-15	3.66374e-15	3.9968e-14	1.59872e-14	1.24345e-14	1.75771e-12
0.05	2.26485e-14	6.21725e-15	2.84217e-13	3.19744e-14	3.01981e-14	4.99889e-12
0.025	1.25677e-13	1.5099e-14	1.29319e-12	7.10543e-14	6.50591e-14	5.63771e-12
0.0125	1.58851e-12	2.84217e-14	9.9476e-12	1.56319e-13	1.45661e-13	7.12008e-12
0.00625	3.90799e-12	2.38281e-11	3.81561e-11	2.0269e-10	9.92445e-09	1.01445e-08

Table 3.2:  $L^\infty$ -error of divergence for different mesh sizes  $h$ .

The  $L^2$ - and  $L^\infty$ -error of the divergence for different mesh sizes  $h$  is shown in Table 3.1 and Table 3.2, respectively. We see that both stabilized methods preserve the incompressibility condition. For the last iteration, i.e.  $h = 0.00625$ , we had to use MUMPS instead of UMFPACK, resulting in significantly worse divergence error.

### 3.1.1. Influence of Lagrange multipliers on the divergence condition

We study how different approaches of prescribing the constant in the pressure in case of Dirichlet boundary conditions can influence the numerical results. The convergence order and the scaling of the condition number are not influenced. Therefore, we here focus on the divergence error. We compare the standard way of imposing the mean value for the pressure and the functions in the test space with the new approach presented in Section 2.6. We use the pair  $\mathbf{BDM}_1 \times Q_0$  with  $\lambda_{\mathbf{u}} = 4 \cdot 10^3$  for Method NC and the triple  $P_1 \times$

$\mathbf{RT}_0 \times Q_0$  for Method C with  $\lambda_u = 8 \cdot 10^2$ , i.e., the lowest order versions. We choose the macro stabilization parameter  $\delta = 0.5$ .

We see in the left panel of Figure 3.3 how the  $L^\infty$ -error of the divergence is incorrect by exactly the value of the Lagrange multiplier. Table 3.3 showcases the  $L^\infty$ -errors for different mesh sizes  $h$ . We clearly see that in the unfitted setting the imposition of the mean value of functions  $q$  in the test space, as it is usually done, destroys the divergence-free property of the  $\mathbf{H}^{\text{div}}$ -conforming finite element spaces. On the other hand, prescribing the constant in the pressure following the proposed approach, see Section 2.6, both unfitted discretizations result in discrete velocity fields with errors in the divergence of the order of machine epsilon.

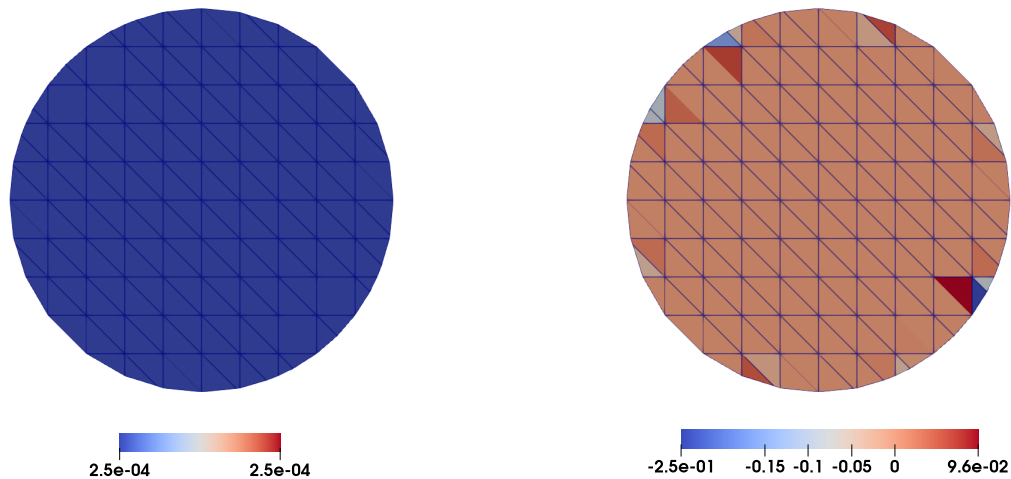


Figure 3.3: Example 1: Divergence heatmaps using the element pair  $\mathbf{BDM}_1 \times Q_0$  for  $h = 0.05$ . Left: The error in the divergence when a standard Lagrange multiplier is used to enforce the pressure mean. The error is constant  $2.5 \cdot 10^{-4}$  which is equal to the value of the Lagrange multiplier. Right: The error in the divergence using the pressure stabilization  $s_p$ . The divergence-free property of the  $\mathbf{H}^{\text{div}}$ -conforming elements we use are destroyed by the standard ghost penalty stabilization  $s_p$ .

$h$	Method NC (BDM1): no stabilization	Method NC (BDM1): $\delta = 0.5$ , standard Lagrange multiplier	Method NC (BDM1): $\delta = 0.5$	Method C (RT0): no stabilization	Method C (RT0): $\delta = 0.5$ , standard Lagrange multiplier	Method C (RT0): $\delta = 0.5$
0.1	5.10703e-15	0.000251855	2.66454e-14	3.55271e-15	0.00108032	2.83107e-14
0.05	2.26485e-14	0.000135779	3.10862e-14	4.44089e-15	0.000633879	7.08322e-14
0.025	1.25677e-13	7.03835e-05	1.86962e-13	1.06581e-14	0.000339477	7.19425e-14
0.0125	1.58851e-12	3.58296e-05	5.50671e-13	2.4869e-14	0.000175661	1.18017e-13

Table 3.3:  $L^\infty$ -error of divergence for different mesh sizes  $h$ . Comparing the proposed method with setting the Lagrange multiplier in the standard way.

### 3.1.2. The importance of correct stabilization

The choice of stabilization terms is another important aspect which influences the behaviour of both methods. Consider for instance Method NC. Exchanging the stabilization term  $s_b(\cdot, \cdot)$  acting on  $\mathbf{V}_{k,h} \times Q_{\hat{k},h}$  with the pressure stabilization term  $s_p(\cdot, \cdot)$  acting on  $Q_{\hat{k},h} \times Q_{\hat{k},h}$ , which has been used in most previous work, ruins the incompressibility. See the right panel of Figure 3.3 for heatmap of the error; The error in the divergence is large in the vicinity of edges where stabilization is applied. A detailed comparison in the case of the Darcy equations was given in [10]. The  $L^\infty$ -errors we observe here for the Stokes problem are actually

worse. In Table 3.4 we show the divergence error when the proposed stabilization  $s_b(\cdot, \cdot)$  is used compared to the commonly used stabilization term  $s_p(\cdot, \cdot)$ .

$h$	Method NC (BDM1): $\delta = 0.5$ , with $s_p$	Method NC (BDM1): $\delta = 0.5$
0.1	0.687812	2.66454e-14
0.05	0.562762	3.10862e-14
0.025	0.429216	1.86962e-13
0.0125	0.193141	5.50671e-13

Table 3.4:  $L^\infty$ -error of divergence for different mesh sizes  $h$ . Comparison of the proposed discretization using the stabilization terms  $s_b(\mathbf{v}, p)$ , with the pressure stabilization  $s_p(p, q)$  often used in connection with CutFEM. Results are shown for Method NC with  $\mathbf{BDM}_1 \times Q_0$ .

### 3.1.3. Method C, different boundary conditions and choice of stabilization

We make a comparison between the present version of Method C, i.e.,  $(\tau_w, 0, \tau_a)$  with  $\gamma_a = 1$  and  $\lambda_{\mathbf{u}} = 800$ , with the version  $(0, \tau_m, 0)$ . We compare the different choices of stabilization terms both for Dirichlet boundary conditions (1.3), and for the alternative boundary conditions (2.55).

First consider the Dirichlet boundary conditions (1.3). For the  $(0, \tau_m, 0)$ -variant we take  $\tau_b = \tau_m = 2$ ,  $\delta = 1$ , and  $\lambda_{\mathbf{u}} = 40$ . The parameter  $\lambda_{\mathbf{u}}$  is chosen differently for each variant in order to achieve as close to optimal behaviour as possible. This results in two versions of the unstabilized method, one with  $\lambda_{\mathbf{u}} = 40$  and one with  $\lambda_{\mathbf{u}} = 800$ . In the right panel of Figure 3.4 we see not much difference between the two versions in terms of their velocity convergence. The pressure convergence is best for the present version of Method C  $(\tau_w, 0, \tau_a)$  with  $\gamma_a = 1$ . In Figure 3.5 we see the condition number as a function of mesh size  $h$ . The condition number is controlled with both stabilization variants but is a bit larger for the current variant due to a larger penalty parameter, i.e.,  $\lambda_{\mathbf{u}} = 800$  (compared to  $\lambda_{\mathbf{u}} = 40$ ). The divergence is not impacted in any remarkable

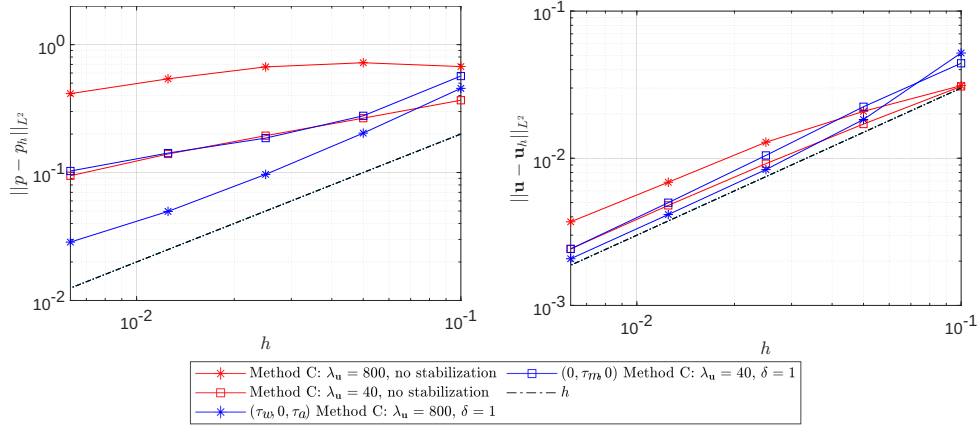


Figure 3.4: Example 1: Method C  $(\tau_w, 0, \tau_a)$  vs.  $(0, \tau_m, 0)$  [Dirichlet BC], pressure and velocity errors compared for the lowest order triple  $P_1 \times \mathbf{RT}_0 \times Q_0$ . Left: The  $L^2$ -error of the pressure versus mesh size  $h$ . Right: The  $L^2$ -error of the velocity field versus mesh size  $h$ .

way; the errors have the same order of magnitude for each mesh size  $h$ .

We study the performance of Method C for the Stokes equations with boundary conditions (2.55), that is  $\mathbf{u} \cdot \mathbf{t} = u_0$  and  $p = p_0$  at the boundary. With these boundary conditions there is no uniqueness issue for the pressure, so we do not have to introduce any Lagrange multiplier. Now the most natural choice of stabilization for Method C is  $(0, \tau_m, 0)$  since there is no  $\mathbf{A}$ -block. We compare this variant with the  $(\tau_w, 0, \tau_a)$ -variant of the previous subsection. The stabilization parameters are taken to be  $\tau_w = \tau_m = \tau_a = \tau_b = 1$  and the macro stabilization parameter  $\delta = 0.25$ .

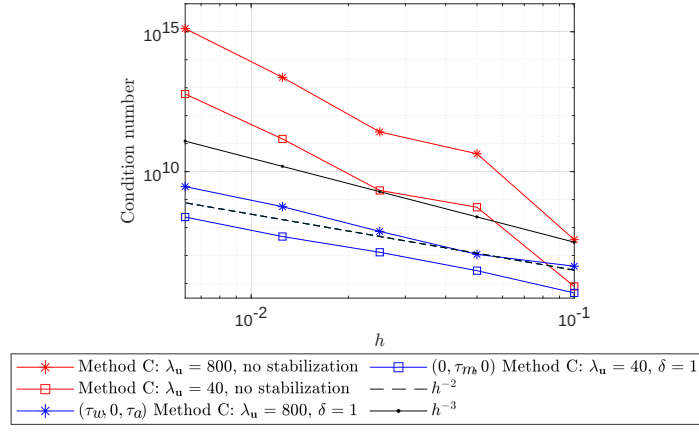


Figure 3.5: Example 1: Method C  $(\tau_w, 0, \tau_a)$  vs.  $(0, \tau_m, 0)$  [Dirichlet BC], the 1-norm condition number versus mesh size  $h$  for the lowest order triple  $P_1 \times \mathbf{RT}_0 \times Q_0$ .

We can see in Figure 3.6 that both variants of stabilization perform optimally in all respects for the lowest order elements, order  $k = 0$ , i.e., using the triple  $P_1 \times \mathbf{RT}_0 \times Q_0$ . However, for  $k = 1$ , using the triple  $P_2 \times \mathbf{RT}_1 \times Q_1$  we see in the right panel of Figure 3.6 that variant  $(0, \tau_m, 0)$  behaves better with respect to the scaling of the condition number with mesh size. Increasing the parameter  $\delta > 0.25$  is in fact not enough to save the scaling issues of variant  $(\tau_w, 0, \tau_a)$  with these boundary conditions. Hence which stabilization terms one should include in Method C depends on the type of boundary conditions.

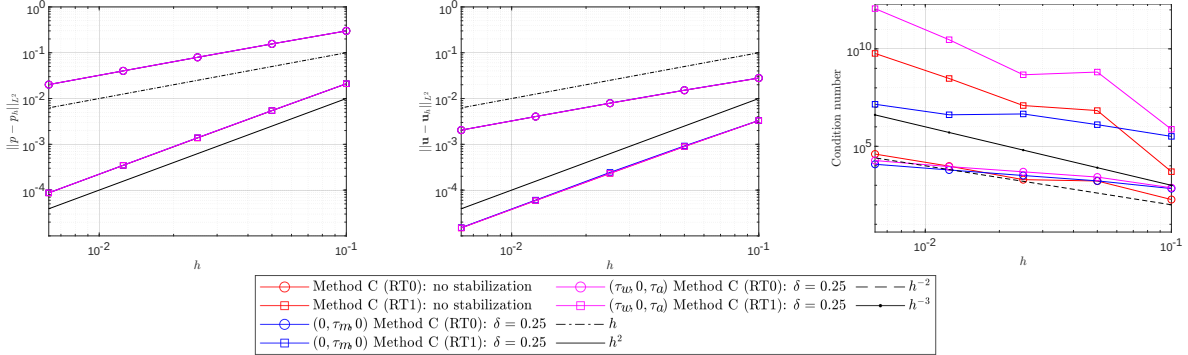


Figure 3.6: Example 1: Method C  $(\tau_w, 0, \tau_a)$  vs.  $(0, \tau_m, 0)$  [alt. BC], pressure and velocity errors and condition numbers for both element triples  $P_1 \times \mathbf{RT}_0 \times Q_0$  and  $P_2 \times \mathbf{RT}_1 \times Q_1$ . Left:  $L^2$ -error of pressure. Middle:  $L^2$ -error of velocity versus mesh size  $h$ . Right: The 1-norm condition number versus mesh size  $h$ .

### 3.2. Example 2 - Coriolis force, pressure-robustness

We consider an example from [1], where for  $\mathbf{u} = \mathbf{u}(x, y)$  the momentum balance is modified with a Coriolis

force  $\boldsymbol{\lambda} \times \mathbf{u} = \Lambda \begin{bmatrix} 0 \\ 0 \\ 1 \end{bmatrix} \times \begin{bmatrix} u_1 \\ u_2 \\ 0 \end{bmatrix}$ ,  $\Lambda > 0$ , so that we consider the problem

$$-\operatorname{div}(\mu \nabla \mathbf{u} - p \mathbf{I}) + \Lambda \begin{bmatrix} -u_2 \\ u_1 \end{bmatrix} = 0. \quad (3.2)$$

In the weak formulations of Method NC and Method C, the term  $(\Lambda \begin{bmatrix} -u_2 \\ u_1 \end{bmatrix}, \boldsymbol{\nu})_\Omega$  is added in (2.26) and (2.44).

For standard boundary-fitted FEM, pressure-robustness in a discretization of Stokes and Navier-Stokes is the following property (which we only describe very briefly, see [1] for details): A modification of the data by a gradient term should only impact the pressure solution, i.e.

$$\mathbf{f} \mapsto \mathbf{f} + \nabla\psi \implies (\mathbf{u}_h, p_h) \mapsto (\mathbf{u}_h, p_h + \psi). \quad (3.3)$$

In the present example, since  $\text{curl}(\boldsymbol{\lambda} \times \mathbf{u}) = 0$ , there is a potential function  $\psi$  such that  $\nabla\psi = \boldsymbol{\lambda} \times \mathbf{u}$ , and therefore the term  $\boldsymbol{\lambda} \times \mathbf{u}$  should not impact the velocity in a pressure-robust scheme.

A necessary condition for (3.3) is that  $\text{div}\mathbf{V}_{k,h} \subset Q_{k,h}$ , and a question is whether or not this also holds in the unfitted setting.

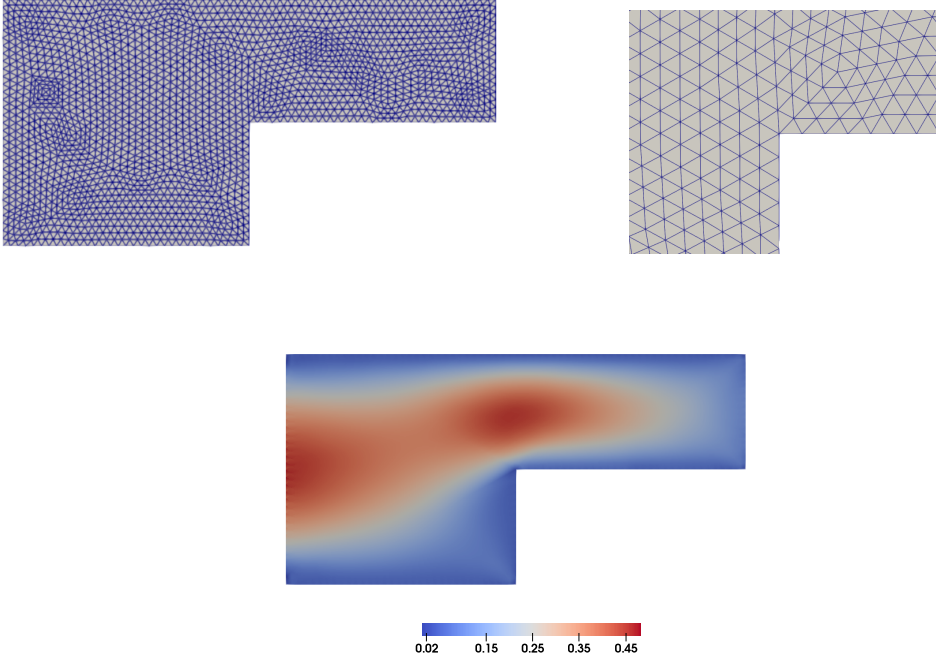


Figure 3.7: Example 2: Computations on a boundary-fitted mesh, with  $h = \max_{T \in \mathcal{T}_h} h_T = 0.0742408$ . Top: The computational mesh. In the right panel we zoom in at one of the corners. Bottom: Magnitude of the approximate velocity field using the method of [18] with the element pair  $\mathbf{BDM}_1 \times Q_0$ .

We take  $\mu = 1$  and  $\Lambda = 100$ . The macro-stabilization parameter is  $\delta = 1$ . For Method NC we divide up the penalty  $\lambda_{\mathbf{u}}$  such that we have one for the tangential component  $\lambda_{\mathbf{u},\mathbf{t}} = \lambda_t = 4$  and one for the normal component  $\lambda_{\mathbf{u},\mathbf{n}} = 8e - 1$ .

The geometry is an L-shaped domain  $[0, 2] \times [0, 2] \cup [2, 4] \times [1, 2]$ , see the top panel of Figure 3.7 for a fitted mesh of it. Method NC without stabilization terms applied to the Stokes problem using a fitted mesh gives the same discretization as the method of [11, 18]. We choose  $h = \max_{T \in \mathcal{T}_h} h_T = 0.0742408$ . The approximated velocity is shown in the bottom panel of Figure 3.7. The same figure is obtained when the  $\boldsymbol{\lambda} \times \mathbf{u}$  term is not present; so the method is numerically pressure-robust.

Changing to a uniform unfitted mesh shown in Figure 3.8, we see that Method NC (2.68) is also numerically pressure-robust in the same way, see left panel of Figure 3.9. If we on the other hand impose the mean value of functions in  $Q_{k,h}$  as in (2.64), which is the standard way, and stabilizing the pressure using  $s_p$ , which is commonly used in connection with CutFEM [23, 4], the pressure-robustness is completely lost. The Coriolis force has a huge impact on the velocity solution, see the right panel of Figure 3.9. Note apart from the sudden rotational flow also the change in magnitude of the velocity field.



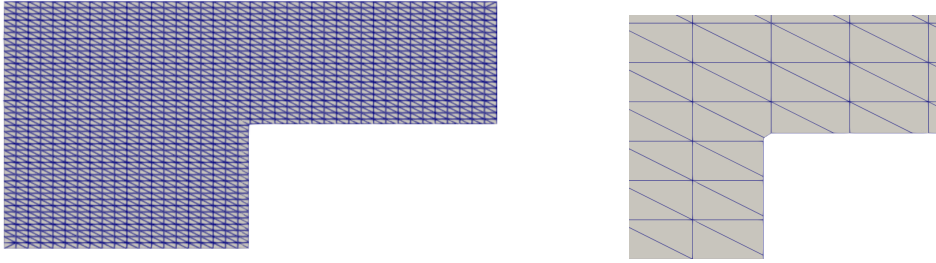


Figure 3.8: Example 2: The uniform unfitted mesh. In the right panel a zoom of the unfitted part  $\Sigma = \{(x, y) \in \partial\Omega : x = 2 \text{ or } y = 1\}$  is shown.

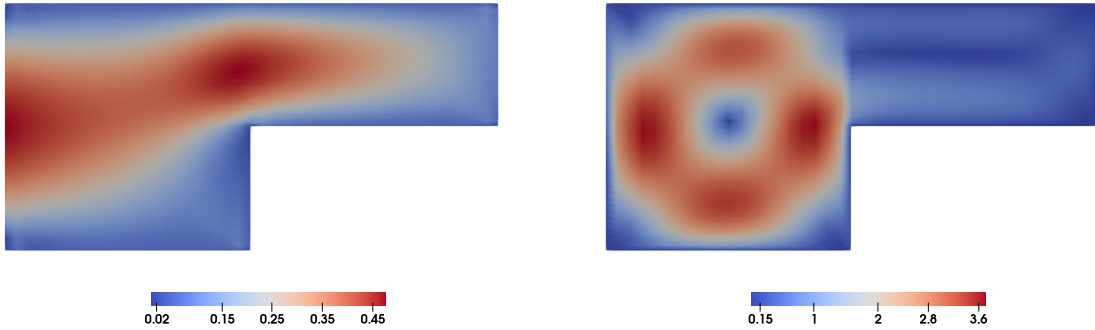


Figure 3.9: Example 2: The magnitude of the approximate velocity field using Method NC with the element pair  $\mathbf{BDM}_1 \times Q_0$  and macro-stabilization parameter  $\delta = 1$ . Left: Results using the proposed discretization. Right: Results using a standard Lagrange multiplier approach to set the mean value of functions in  $Q_{k,h}$  and replacing the stabilization term  $s_b$  with  $s_p$ .

With Method C (2.70) the situation is almost entirely analogous, see Figure 3.10 for Method C  $(\tau_w, 0, \tau_a)$  with  $\gamma_a = 1$  applied to the unfitted mesh. We see however in the right panel that Method C is more sensitive with respect to this kind of disturbance, by a whole order of magnitude.

Of greatest detrimental effect to pressure-robustness in this example seems to be the standard Lagrange multiplier technique of (2.64) for prescribing the constant in the pressure in case of Dirichlet boundary conditions. Changing only the stabilization  $s_b$  to  $s_p$  changes the magnitude of the velocity by a smaller amount, and the macroscopic behaviour is not altered as much as not setting the Lagrange multiplier correctly. However, as  $\Lambda$  increases so does the velocity error, and consequently there is a threshold of  $\Lambda$  after which changing only  $s_b$  to  $s_p$  also breaks the solution akin to Figures 3.9 and 3.10.

#### 4. Conclusion

We developed two cut finite element methods for the Stokes equations. For both methods the divergence-free condition holds pointwise and numerical experiments show that both schemes are pressure-robust. To achieve divergence-free velocity approximations we utilize  $\mathbf{H}^{\text{div}}$ -conforming elements but develop both appropriate ghost penalty stabilization terms as well as a new approach to determine a unique pressure approximation. The pressure only being determined up to a constant in case of Dirichlet boundary conditions represented a major difficulty since we could not obtain pointwise divergence-free velocity approximations

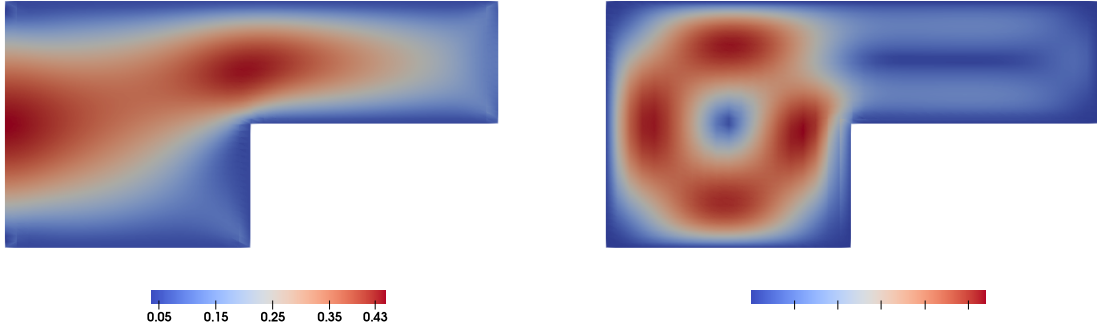


Figure 3.10: Example 2: The magnitude of the approximate velocity field using Method C with the element triple  $P_2 \times \mathbf{RT}_1 \times Q_1$  and macro-stabilization parameter  $\delta = 1$ . Left: Results using the proposed discretization. Right: Results using a standard Lagrange multiplier approach to set the mean value of functions in  $Q_{k,h}$  and replacing the stabilization term  $s_b$  with  $s_p$ .

on unfitted meshes using the standard approach of setting the mean value of the functions in the pressure space using a Lagrange multiplier. The mixed Lagrange multipliers introduced in Section 2.6 is our proposed solution to the problem.

We presented a cut finite element method based on the non-conforming method of [11] that we refer to as Method NC, see Section 2.4 and a CutFEM for the vorticity-velocity-pressure formulation of the Stokes problem, that we refer to as Method C, see Section 2.5. With Method C comes several possibilities of appropriate stabilization terms, and it seems from our numerical studies that the version of choice depends on the boundary conditions. For the Stokes problem with Dirichlet boundary conditions the best choice was  $(\tau_w, 0, \tau_a)$ . This variant gave optimal convergence order both for the velocity and the pressure and the condition number scaling with respect to mesh size was as for standard finite element methods. Method NC gave optimal results with the  $\mathbf{BDM}$ -family for its velocity space. It is hard to directly compare the two methods since one could in theory compare  $\mathbf{BDM}_1 \times Q_0$  of Method NC with both  $P_1 \times \mathbf{RT}_0 \times Q_0$  and  $P_2 \times \mathbf{RT}_1 \times Q_1$  of Method C, depending on if one wants to match the pressure convergence or the velocity convergence.

If we compare  $\mathbf{BDM}_k \times Q_{k-1}$  with  $P_k \times \mathbf{RT}_{k-1} \times Q_{k-1}$ , a degree-of-freedom count per element gives

$$[\text{Method NC} - \text{Method C}] : (k+1)(k+2) + \frac{k(k+1)}{2} - \left( \frac{(k+1)(k+2)}{2} + k(k+2) + \frac{k(k+1)}{2} \right) \quad (4.1)$$

$$= \frac{k+2 - k(k+2)}{2} = \frac{(1-k)(k+2)}{2}. \quad (4.2)$$

Thus, there are  $\frac{(k-1)(k+2)}{2}$ ,  $k > 1$ , more DOFs per element in Method C than in Method NC coming from the extra Lagrange space of the vorticity variable. The discrepancy is of course larger if we compare  $\mathbf{BDM}_k \times Q_{k-1}$  with  $P_{k+1} \times \mathbf{RT}_k \times Q_k$  as we did in Example 1. The above count is slightly pessimistic in aggregate since the DOFs are shared between elements. However, the interior edge terms in Method NC change the sparsity pattern of the system matrix. In our implementation, the assembly of Method NC is slightly slower than Method C even when comparing  $\mathbf{BDM}_k \times Q_{k-1}$  with  $P_{k+1} \times \mathbf{RT}_k \times Q_k$ .

*Acknowledgement.* This research was supported by the Swedish Research Council Grant No. 2018-04192, 2022-04808, and the Wallenberg Academy Fellowship KAW 2019.0190.

## References

- [1] V. John, A. Linke, C. Merdon, M. Neilan, L. G. Rebholz, On the divergence constraint in mixed finite element methods for incompressible flows, *SIAM Review* 59 (3) (2017) 492–544. doi:10.1137/15M1047696.
- [2] T. Frachon, S. Zahedi, A cut finite element method for incompressible two-phase Navier-Stokes flows, *J. Comput. Phys.* 384 (2019) 77–98.
- [3] T. Frachon, S. Zahedi, A cut finite element method for two-phase flows with insoluble surfactants, *Journal of Computational Physics* 473 (2023) 111734.
- [4] P. Hansbo, M. G. Larson, S. Zahedi, A cut finite element method for a Stokes interface problem, *Appl. Numer. Math.* 85 (2014) 90–114.
- [5] M. Kirchhart, S. Gross, A. Reusken, Analysis of an XFEM discretization for Stokes interface problems, *SIAM Journal on Scientific Computing* 38 (2) (2016) A1019–A1043.
- [6] E. Burman, P. Hansbo, Fictitious domain methods using cut elements: III. A stabilized Nitsche method for Stokes problem, *ESAIM: M2AN* 48 (3) (2014) 859–874.
- [7] A. Massing, M. Larson, A. Logg, M. Rognes, A stabilized Nitsche fictitious domain method for the Stokes problem, *Journal of Scientific Computing* 61 (3) (2014) 604–628.
- [8] E. Burman, Ghost penalty, *C. R. Acad. Sci. Paris, Ser. I* 348 (21-22) (2010) 1217 – 1220.
- [9] H. Liu, M. Neilan, M. Olshanskii, A cutfem divergence-free discretization for the Stokes problem, *ESAIM: M2AN* 57 (1) (2023) 143–165.
- [10] T. Frachon, P. Hansbo, E. Nilsson, S. Zahedi, A divergence preserving cut finite element method for Darcy flow, *arXiv:2205.12023* (2022).
- [11] J. Wang, X. Ye, New finite element methods in computational fluid dynamics by H(Div) elements, *SIAM Journal on Numerical Analysis* 45 (3) (2007) 1269–1286.
- [12] B. Cockburn, G. Kanschat, D. Schötzau, A note on Discontinuous Galerkin divergence-free solutions of the Navier–Stokes equations, *Journal of Scientific Computing* 31 (2007) 61–73. doi:10.1007/s10915-006-9107-7.
- [13] F. Dubois, Vorticity–velocity–pressure formulation for the Stokes problem, *Mathematical Methods in the Applied Sciences* 25 (13) (2002) 1091–1119.
- [14] M. Hanot, An arbitrary order and pointwise divergence-free finite element scheme for the incompressible 3d navier-stokes equations, *arXiv preprint arXiv:2106.05146* (2021).
- [15] M. G. Larson, S. Zahedi, Conservative cut finite element methods using macro-elements, <http://dx.doi.org/10.2139/ssrn.4391680> (2023).
- [16] F. Brezzi, M. Fortin, *Mixed and hybrid finite element methods*, Springer Science & Business Media, 2012.
- [17] D. Boffi, F. Brezzi, M. Fortin, *Mixed finite element methods and applications*, Vol. 44, Springer, 2013.
- [18] J. Wang, Y. Wang, X. Ye, A robust numerical method for Stokes equations based on divergence-free H(div) finite element methods, *SIAM Journal on Scientific Computing* 31 (4) (2009) 2784–2802.
- [19] D. Arnold, R. Falk, R. Winther, Preconditioning in H(div) and applications, *Math. Comp* 66 (1997) 957–984.

- [20] Defelement website (de rham families), <https://defelement.com/families/index.html>.
- [21] Periodic table of finite elements, <https://www-users.cse.umn.edu/~arnold/femtable/>.
- [22] Cutfem-library, <https://github.com/CutFEM/CutFEM-Library>.
- [23] R. Puppi, A cut finite element method for the Darcy problem, arXiv:2111.09922 (2021).